

# Description of neutron-rich odd-mass krypton isotopes within the interacting boson-fermion model based on the Gogny energy density functional

K. Nomura,<sup>1</sup> R. Rodríguez-Guzmán,<sup>2</sup> and L. M. Robledo<sup>3,4</sup>

<sup>1</sup>*Physics Department, Faculty of Science, University of Zagreb, HR-10000 Zagreb, Croatia*

<sup>2</sup>*Physics Department, Kuwait University, 13060 Kuwait, Kuwait*

<sup>3</sup>*Center for Computational Simulation, Universidad Politécnica de Madrid, Campus de Montegancedo, Boadilla del Monte, 28660-Madrid, Spain*

<sup>4</sup>*Departamento de Física Teórica, Universidad Autónoma de Madrid, E-28049 Madrid, Spain*

(Dated: February 17, 2022)

The low-lying structure of neutron-rich odd-mass Kr isotopes is studied within the interacting boson-fermion model (IBFM) based on the Gogny-D1M energy density functional (EDF). The  $(\beta, \gamma)$ -deformation energy surfaces, spherical single-particle energies and occupation probabilities of the odd-mass systems are obtained using the constrained Hartree-Fock-Bogoliubov (HFB) approximation. Those quantities are used as a microscopic input to determine most of the parameters of the IBFM Hamiltonian. The remaining parameters are specifically tailored to the experimental spectrum for each of the studied odd-mass nuclei. A gradual structural evolution is predicted for the odd-mass isotopes  $^{87-95}\text{Kr}$  as a function of the nucleon number which, agrees well with the gradual growth of collectivity observed experimentally in the neighboring even-even isotopes.

## I. INTRODUCTION

The neutron-rich nuclei in the mass region  $A \approx 100$  exhibit a rich variety of nuclear structure phenomena, such as quantum phase transitions [1] associated to ground state shape evolution or the presence of shape coexistence [2]. In particular, the neutron-rich Kr ( $Z = 36$ ) isotopes have recently attracted much attention because of their shape evolution with neutron number. For instance, at variance with the neighboring even-even Sr ( $Z = 38$ ) and Zr ( $Z = 40$ ) nuclei, where a rapid structural change has been suggested around  $N = 60$  [3–5], the shape transition is rather moderate in the Kr isotopic chain [6]. A number of experiments, using radioactive beams, have already been devoted to the study and characterization of the properties of neutron-rich even-even Kr isotopes [6–10]. Nuclei of this region of the nuclear chart have also been studied within several theoretical frameworks (see, for example, [3, 6, 8–15], and references therein).

Spectroscopic data are also available for neutron-rich odd-mass Kr nuclei like  $^{91}\text{Kr}$  [16],  $^{93}\text{Kr}$  [17] and  $^{95}\text{Kr}$  [18]. However, from a theoretical point of view, those odd-mass systems have not yet been as much studied as the even-even ones. This is because the description of odd-mass systems tends to be cumbersome, as it requires to treat both the single-particle and collective degrees of freedom on an equal footing [19]. For example, within the energy density functional (EDF) framework, the need to consider blocked one-quasiparticle wave functions [20] is what complicates the description of odd-mass nuclei. Those blocked wave functions break time-reversal invariance which requires the evaluation of time-odd fields to solve the corresponding Hartree-Fock-Bogoliubov (HFB) equations. Furthermore, due to the (nonlinear) self-consistent character of the HFB equations, there is no guarantee to obtain the lowest energy solution by blocking the quasiparticle with the lowest one-quasiparticle

excitation energy of the neighboring even system. Therefore, the blocking procedure has to be repeated starting from several different low-lying one-quasiparticle states of the neighboring nuclei. From what has already been mentioned, it is clear that alternative routes should be explored to afford the computational cost of the EDF description of odd-mass nuclei. Within this context, the so called Equal Filling Approximation (EFA) [11, 21] has emerged as a useful tool for microscopic studies of odd-mass nuclei (see, for example, [22, 23], and references therein). Though the HFB-EFA alleviates the computational effort required to study medium and heavy odd-mass nuclei, it still provides limited access to their spectroscopic properties.

In this paper, we consider the spectroscopy of neutron-rich odd-mass Kr isotopes. To this end, we have resorted to a method [24] that combines the advantages of both the energy density functional (EDF) framework and the ones of the interacting boson-fermion model (IBFM) [25]. The deformation energy surfaces for the neighboring even-even nuclei as well as the single-particle energies and occupation probabilities for the odd-mass systems, are computed using the (constrained) self-consistent mean-field (SCMF) approximation. Those quantities are then used as a microscopic input to determine most of the corresponding IBFM Hamiltonian. A few remaining parameters, i.e., coupling constants for the boson-fermion interaction, are then specifically fitted to reproduce experimental spectra in each odd-mass nucleus. The method allows a systematic and efficient description of the spectroscopic properties of odd-mass nuclei in various mass regions [26, 27]. In this study, we have considered  $^{87,89,91,93,95}\text{Kr}$  which are the heaviest odd-mass Kr isotopes for which experimental data for excitation spectra are available. Calculations for even-even Kr isotopes, have already been carried out in Refs. [6, 8, 15] using an interacting boson model (IBM) based on the Gogny-EDF. It has been shown, that the even-even nu-

clei  $^{86-94}\text{Kr}$  undergo a gradual transition from nearly spherical to  $\gamma$ -soft and then to oblate shapes with increasing neutron number. Those results point to a moderate growth of collectivity as observed in the experimental data [6].

Recent experimental studies as well as EDF-based calculations [12, 15] have suggested that shape coexistence is likely to occur in the even-even Kr isotopes beyond the mass number  $A = 96$ . In order to study those nuclei, intruder configurations associated with different nuclear shapes have to be introduced within the IBM formalism [8, 15]. However, as shown below, shape coexistence plays a minor role for the even-even core nuclei  $^{86-94}\text{Kr}$  considered in this work and therefore there is no need in our IBFM calculations to consider intruder configurations as it would be the case for those isotopes with  $A \geq 96$ .

The low-lying structure of the  $N = 53$  isotones  $^{85}\text{Ge}$ ,  $^{87}\text{Se}$  and  $^{89}\text{Kr}$  has been studied in Ref. [28] within the IBFM-2 phenomenology. Aside from that study, and to the best of our knowledge, the IBFM framework has rarely been applied to the mass region  $A \approx 100$  beyond the neutron number  $N = 50$ . Perhaps, this is because only recently experimental data have become available for both even-even and odd-mass nuclei in this region. Therefore, one of the aims of this study will be to test the validity of employed theoretical framework in the description of neutron-rich odd-mass isotopes in the mass region  $A \approx 100$ .

The paper is organized as follows. In Sec. II, we briefly describe the theoretical scheme used in this work. In Sec. III, we review some key results for even-even Kr isotopes. Then in Sec. IV, we discuss the spectroscopic properties for odd-mass Kr nuclei. In particular, we consider the systematic of the low-energy yrast levels, detailed level schemes for individual nuclei,  $B(E2)$  and  $B(M1)$  transition strengths, spectroscopic quadrupole and magnetic moments. Finally, Sec. V is devoted to concluding remarks and work perspectives.

## II. THEORETICAL PROCEDURE

In this section we briefly outline the theoretical framework used in this study. For a more detailed account, the reader is referred to Refs. [24, 26].

The IBFM Hamiltonian  $\hat{H}_{\text{IBFM}}$  consists of the neutron-proton IBM (IBM-2) Hamiltonian  $\hat{H}_{\text{B}}$ , the single-particle fermion Hamiltonian  $\hat{H}_{\text{F}}$ , and the boson-fermion interaction term  $\hat{H}_{\text{BF}}$

$$\hat{H}_{\text{IBFM}} = \hat{H}_{\text{B}} + \hat{H}_{\text{F}} + \hat{H}_{\text{BF}}. \quad (1)$$

The IBM-2 term  $\hat{H}_{\text{B}}$  is comprised of the neutron (proton)  $s_\nu$  and  $d_\nu$  ( $s_\pi$  and  $d_\pi$ ) bosons, which are associated with collective pairs of valence neutrons (protons) with spin  $J = 0^+$  and  $2^+$ , respectively [29], outside the  $^{78}\text{Ni}$  double-magic core. We have used the same Hamiltonian

$\hat{H}_{\text{B}}$  as in Refs. [6, 8], where the  $(\beta, \gamma)$ -deformation energy surfaces have been computed using the constrained Hartree-Fock-Bogoliubov (HFB) method [30] based on the parametrization D1M of the Gogny-EDF [31, 32]. The corresponding mean-field  $(\beta, \gamma)$ -deformation energy surfaces are then mapped onto the expectation value of the IBM-2 Hamiltonian [33, 34]. This procedure determines the values of the Hamiltonian parameters (see, [8]). For the fermion valence space, we have taken the  $3s_{1/2}$ ,  $2d_{3/2}$ ,  $2d_{5/2}$ , and  $1g_{7/2}$  orbitals of the whole neutron major shell  $N = 50 - 82$  to describe positive-parity states in the studied odd-mass Kr nuclei. Since there is no experimental information about negative-parity states for the considered odd-mass Kr nuclei, we restrict our discussion to the positive-parity ones in this paper.

The  $\hat{H}_{\text{BF}}$  interaction term is taken from [25]:

$$\hat{H}_{\text{BF}} = \Gamma_\nu \hat{Q}_\pi^{(2)} \cdot \hat{q}_\nu^{(2)} + \Lambda_\nu \hat{V}_{\pi\nu} + A_\nu \hat{n}_{d\nu} \hat{n}_\nu. \quad (2)$$

The first term represents the quadrupole dynamical term, given by the product of a strength constant  $\Gamma_\nu$  times the boson quadrupole operator for proton bosons  $\hat{Q}_\pi^{(2)}$  times the fermion quadrupole operator for the odd neutron  $\hat{q}_\nu^{(2)}$ . The latter is given by

$$\hat{q}_\nu^{(2)} = \sum_{jj'} \gamma_{jj'} (a_{j\nu}^\dagger \times \tilde{a}_{j'\nu})^{(2)}, \quad (3)$$

where  $\gamma_{jj'} = (u_j u_{j'} - v_j v_{j'}) Q_{jj'}$ . The  $\gamma_{jj'}$  matrix element is the product of occupancy factors ( $v_j$  and  $u_j$ ) of the fermion orbitals times the matrix element of the quadrupole operator in the single particle basis  $Q_{jj'} = \langle j || Y^{(2)} || j' \rangle$ . The second term in Eq. (2) is the exchange interaction with strength  $\Lambda_\nu$ . It accounts for the fact bosons are built from nucleon pairs. For the operator  $\hat{V}_{\pi\nu}$  we have used the expression

$$\hat{V}_{\pi\nu} = -(s_\pi^\dagger \tilde{d}_\pi)^{(2)} \cdot \left\{ \sum_{jj'j''} \sqrt{\frac{10}{N_\nu(2j+1)}} \beta_{jj'} \beta_{j''j} : ((d_\nu^\dagger \times \tilde{a}_{j''\nu})^{(j)} \times (a_{j\nu}^\dagger \times \tilde{s}_\nu)^{(j')})^{(2)} : \right\} + (H.c.), \quad (4)$$

where  $\beta_{jj'} = (u_j v_{j'} + v_j u_{j'}) Q_{jj'}$ . As can be seen from Eq. (4),  $\hat{V}_{\pi\nu}$  should be considered when the neutron boson number satisfies  $N_\nu \neq 0$ . Therefore, it is omitted for the semi-magic nucleus  $^{87}\text{Kr}$  for which  $N_\nu = 0$ . The third term in Eq. (2) is the monopole interaction with strength  $A_\nu$ . In the same equation,  $\hat{n}_{d\nu}$  is the number operator for neutron  $d$  bosons. On the other hand,  $n_\nu$  reads

$$\hat{n}_\nu = \sum_j (-\sqrt{2j+1}) (a_{j\nu}^\dagger \times \tilde{a}_{j\nu})^{(0)}. \quad (5)$$

The boson-fermion Hamiltonian  $\hat{H}_{\text{BF}}$  of Eq. (2) can be justified from microscopic considerations [25, 35]: both

TABLE I. The single-particle energies  $\epsilon_j$  (in MeV units) and occupation probabilities  $v_j^2$  of odd neutron at each orbital, and the fitted strength parameters  $\Gamma_\nu$ ,  $\Lambda_\nu$  and  $A_\nu$  (in MeV units) employed in the present study for the odd-mass nuclei  $^{87-95}\text{Kr}$ . Note that the monopole term has not been introduced for the  $2d_{5/2}$  orbital. For details, see the main text.

		$3s_{1/2}$	$2d_{3/2}$	$2d_{5/2}$	$1g_{7/2}$	$\Gamma_\nu$	$\Lambda_\nu$	$A_\nu$
$^{87}\text{Kr}$	$\epsilon_j$	1.766	2.589	0.000	2.753	0.56	-	-
	$v_j^2$	0.011	0.009	0.152	0.007			
$^{89}\text{Kr}$	$\epsilon_j$	1.702	2.722	0.000	2.744	0.80	0.87	0.0
	$v_j^2$	0.042	0.025	0.443	0.022			
$^{91}\text{Kr}$	$\epsilon_j$	1.662	2.830	0.000	2.720	0.80	0.5	-1.2
	$v_j^2$	0.109	0.041	0.705	0.045			
$^{93}\text{Kr}$	$\epsilon_j$	1.672	2.885	0.000	2.657	0.80	2.4	-2.5
	$v_j^2$	0.283	0.080	0.846	0.116			
$^{95}\text{Kr}$	$\epsilon_j$	1.697	2.883	0.000	2.554	0.80	2.4	-1.8
	$v_j^2$	0.463	0.150	0.882	0.240			

the quadrupole dynamical and exchange terms act predominantly between protons and neutrons (i.e., between odd neutron and proton bosons), while the monopole interaction acts between like-particles (i.e., between odd neutron and neutron bosons). The single-particle energies  $\epsilon_j$  and the occupation probabilities  $v_j^2$  for the odd neutron at orbital  $j$ , have been obtained via Gogny-HFB calculations constrained to zero quadrupole moment [26]. The coupling constants  $\Gamma_\nu$ ,  $\Lambda_\nu$  and  $A_\nu$  have been fitted to reproduce the lowest-lying positive-parity levels for each of the considered odd-mass nuclei [24]. Their values, together with  $\epsilon_j$  and  $v_j^2$ , are listed in Table I.

Let us make some remarks on the results shown in Table I:

- For the sake of simplicity, a constant value  $\Gamma_\nu = 0.80$  MeV has been used for  $^{89-95}\text{Kr}$ . We have verified, that the calculated excitation energies are not very sensitive to this parameter.
- The  $\Lambda_\nu$  values for  $^{93,95}\text{Kr}$  are roughly a factor three larger than those for  $^{89,91}\text{Kr}$ . This reflects that the ground state's spin changes from  $^{91}\text{Kr}$  to  $^{93}\text{Kr}$  [16, 36] (see also, Fig. 3).
- For  $^{91,93,95}\text{Kr}$ , the monopole term was not introduced for the  $2d_{5/2}$  orbital. This is because the SCMF single-particle energy of the  $2d_{5/2}$  orbital turned out to be too low ( $\approx 1.7$  MeV) as compared to the one for the  $3s_{1/2}$  orbital.

The diagonalization of the IBFM-2 Hamiltonian provides both excitation energies and wave functions. Those IBFM-2 wave functions have been employed to compute the  $B(E2)$  and  $B(M1)$  transition rates as well as the spectroscopic quadrupole  $Q(J)$  and magnetic  $\mu(J)$  moments. The E2/M1 transition operator is the sum of a

boson and a fermion part

$$\hat{T}^{(E2/M1)} = \hat{T}_B^{(E2/M1)} + \hat{T}_F^{(E2/M1)}. \quad (6)$$

For the boson E2 operator we have assumed the form  $\hat{T}_B^{(E2)} = e_B^\nu \hat{Q}_\nu + e_B^\pi \hat{Q}_\pi$ . The fermion operator  $\hat{T}_F^{(E2)}$  is defined in Ref. [26]. For the proton boson effective charge  $e_B^\pi$  we have used the value  $e_B^\pi = 0.07 eb$  so as to reproduce the experimental  $B(E2; 2_1^+ \rightarrow 0_1^+)$  transition probability for the semi-magic nucleus  $^{86}\text{Kr}$ . We have taken the neutron boson charge  $e_B^\nu$  to be  $e_B^\nu = 0.035 eb = e_B^\pi/2$  in analogy with the shell-model effective charges that satisfy  $e^\pi/e^\nu \approx 2$ . On the other hand, for the neutron effective charge, we have considered the value  $e_F^\nu = 0.5 eb$ . The M1 operator for the boson system reads

$$\hat{T}_B^{(M1)} = \sqrt{\frac{3}{4\pi}} (g_B^\nu \hat{L}_\nu + g_B^\pi \hat{L}_\pi), \quad (7)$$

with  $g_B^\tau$  and  $\hat{L}_\tau$  ( $\tau = \nu, \pi$ ) being the neutron/proton boson  $g$ -factor and angular momentum operator, respectively. We have employed the standard values,  $g_B^\nu = 0 \mu_N$  and  $g_B^\pi = 1.0 \mu_N$ . The fermion M1 operator  $\hat{T}_F^{(M1)}$  is defined in Ref. [26]. For the fermion  $g$ -factors, we have adopted  $g_l = 0 \mu_N$ , and the free value of  $g_s$  has been quenched by 30 %.

### III. RESULTS FOR EVEN-EVEN KR NUCLEI

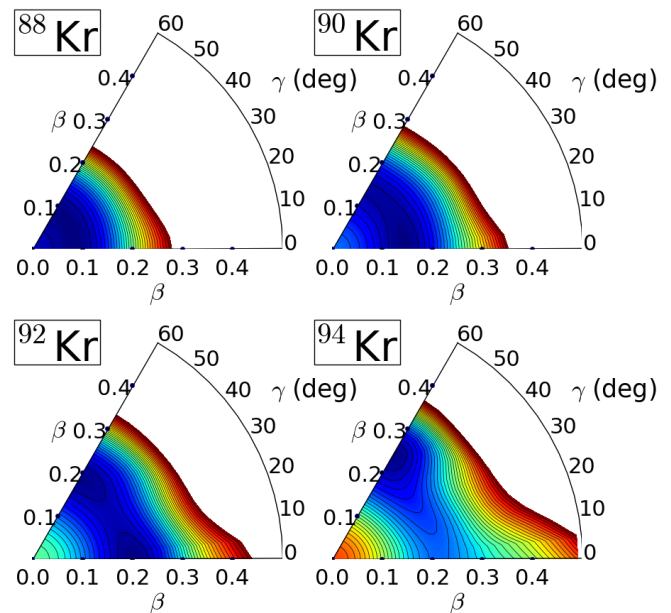


FIG. 1. (Color online) The Gogny-D1M  $(\beta, \gamma)$ -deformation energy surfaces obtained for the nuclei  $^{88,90,92,94}\text{Kr}$ . The energy difference between neighboring contours is 100 keV.

In this section we briefly review some key results already obtained for the even-even isotopes  $^{86-94}\text{Kr}$ .

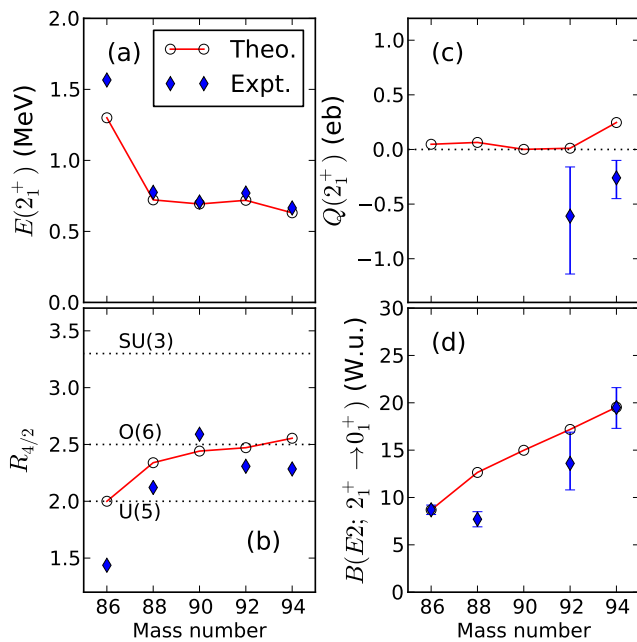


FIG. 2. (Color online) Evolution of the  $2_1^+$  excitation energy  $E(2_1^+)$  [panel (a)], the  $R_{4/2}$  ratio [panel (b)], the spectroscopic quadrupole moment  $Q(2_1^+)$  [panel (c)] and the  $B(E2; 2_1^+ \rightarrow 0_1^+)$  transition strength [panel (d)] as functions of the mass number for the even-even nuclei  $^{86-94}\text{Kr}$ . For details, see the main text.

For a more detailed account, the reader is referred to Refs. [6, 8, 15].

In Figure 1 we have plotted the  $(\beta, \gamma)$  Gogny-D1M energy surfaces obtained for  $^{88-94}\text{Kr}$ . In the case of  $^{86}\text{Kr}$  the energy surface, not included in the figure, exhibits a spherical global minimum. As can be seen from the figure, the global minimum evolves from nearly spherical ( $^{88}\text{Kr}$ ) to pronounced  $\gamma$ -soft ( $^{90,92}\text{Kr}$ ) and then to oblate ( $^{94}\text{Kr}$ ). As already mentioned, for all the nuclei depicted in the figure, no distinct secondary minimum has been obtained.

In Fig. 2 we have plotted the  $2_1^+$  excitation energy  $E(2_1^+)$  [panel (a)], the energy ratio  $R_{4/2} = E(4_1^+)/E(2_1^+)$  [panel (b)], the spectroscopic quadrupole moment  $Q(2_1^+)$  of the  $2_1^+$  state [panel (c)] and the  $B(E2; 2_1^+ \rightarrow 0_1^+)$  transition strength [panel (d)] for the  $^{86-94}\text{Kr}$ . The experimental data, taken from Refs. [6, 8, 36], are also included in the plots for comparisons. The U(5) vibrational ( $R_{4/2} = 2.0$ ), SU(3) rotational ( $R_{4/2} = 3.33$ ) and O(6)  $\gamma$ -soft ( $R_{4/2} = 2.5$ ) IBM [37] limits are indicated in panel (b).

As can be seen from panel (a), the  $2_1^+$  excitation energies predicted within the (mapped) IBM-2 framework nicely follow the experimental ones. Both the theoretical and experimental  $R_{4/2}$ , shown in panel (b), are located in between the U(5) and O(6) limits for most of the nuclei, and gradually increase as functions of the neutron

number. This confirms the smooth onset of collectivity observed experimentally [6]. For the  $N = 50$  nucleus  $^{86}\text{Kr}$ , the experimental  $R_{4/2}$  ratio is much smaller than the vibrational limit of 2.0. Such a feature, typical of spherical nuclei where single-particle dynamics is dominant, cannot be reproduced by the IBM-2, since it is built only on collective pairs.

From panel (c), one sees that the IBM-2  $Q(2_1^+)$  moments are nearly equal to zero for all the nuclei, exception made of  $^{94}\text{Kr}$ . Note, that the Gogny-D1M energy surfaces display nearly spherical and  $\gamma$ -soft minima for  $^{88}\text{Kr}$  and  $^{90,92}\text{Kr}$ , respectively, and an oblate minimum for  $^{94}\text{Kr}$  (see, Fig. 1). The predicted  $Q(2_1^+)$  moments for  $^{92,94}\text{Kr}$  are rather at variance with the experimental ones [8] which exhibit large uncertainties. As can be seen from panel (d), the predicted  $B(E2; 2_1^+ \rightarrow 0_1^+)$  values agree well with the experimental ones.

#### IV. RESULTS FOR ODD-MASS KR NUCLEI

In this section, we discuss the results of our calculations for the studied odd-mass Kr isotopes. In Sec. IV A, we consider the systematic of the low-energy yrast levels. Detailed level schemes are discussed in Sec. IV B. Finally, in Sec. IV C, we discuss electromagnetic properties such as the  $B(E2)$  and  $B(M1)$  transition strengths as well as spectroscopic quadrupole and magnetic moments.

##### A. Systematic of excitation energies

In Fig. 3 we have depicted the excitation spectra for the low-energy positive-parity yrast states in  $^{87-95}\text{Kr}$  as functions of the mass number. In most cases, experimental data are only available for those states in the vicinity of the ground state. As can be seen, the predicted spectra agree reasonably well with the experimental ones. From Fig. 3, one observes a change in the predicted low-lying level structure between  $^{91}\text{Kr}$  and  $^{93}\text{Kr}$ . For example, the  $5/2_1^+$  state is either the ground state ( $^{87,91}\text{Kr}$ ) or in the vicinity of it ( $^{89}\text{Kr}$ ). However, it goes up in energy for  $A > 91$  and for  $^{93,95}\text{Kr}$ , the state  $1/2_1^+$  becomes the ground state. Note, that the neighboring even-even isotopes around  $A = 92$  have been predicted to be in the transitional region between  $\gamma$ -soft and oblate shapes (see, Fig. 1). As shown later, the IBFM-2 wave functions for the ground states of  $^{87,89,91}\text{Kr}$  ( $J = 5/2_1^+$  for  $^{87,91}\text{Kr}$  and  $3/2_1^+$  for  $^{89}\text{Kr}$ ) are predominantly composed of the  $2d_{5/2}$  configuration ( $\approx 90\%$ ) while those of  $^{93,95}\text{Kr}$  with  $J = 1/2_1^+$  are described by a mixture of the  $2d_{3/2}$  ( $\approx 50\%$ ) and  $2d_{5/2}$  ( $\approx 30\%$ ) configurations.

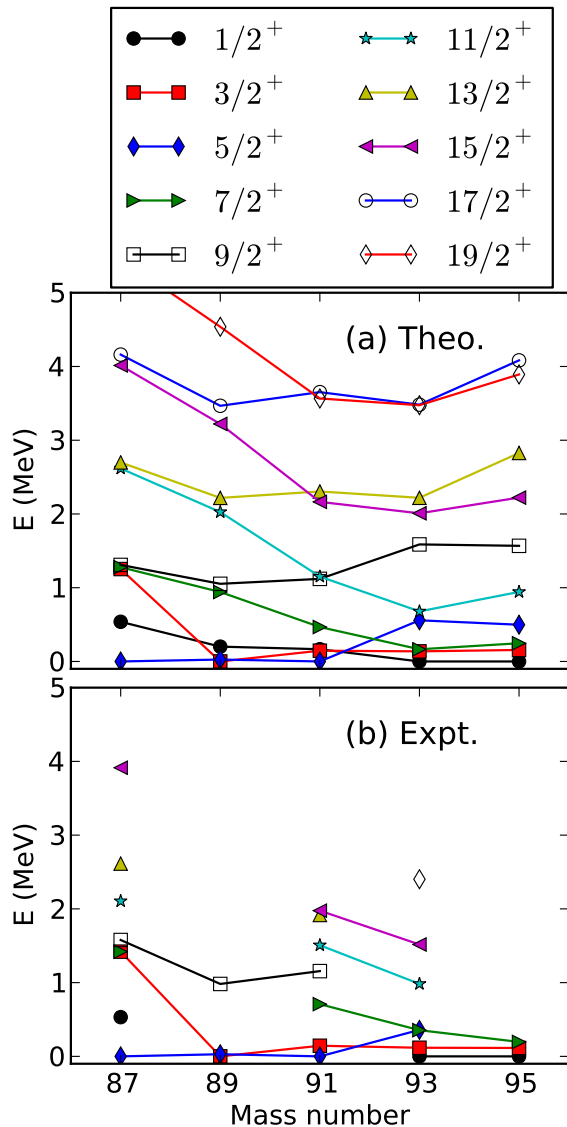


FIG. 3. (Color online) Evolution of the theoretical and experimental [16, 36] excitation energies of the low-lying positive-parity yrast states in the odd-mass nuclei  $^{87-95}\text{Kr}$  as functions of the mass number.

### B. Detailed level schemes

The detailed low-energy level schemes of the positive-parity states are plotted in Figs. 4-8 for  $^{87-95}\text{Kr}$ . Both the experimental and theoretical spectra are shown up to around an excitation energy of 3 MeV. For a given spin  $J$  the lowest two levels are plotted. The fractions of the  $3s_{1/2}$ ,  $2d_{3/2}$ ,  $2d_{5/2}$  and  $1g_{7/2}$  configurations in the IBFM-2 wave functions, corresponding to the low-lying states of the studied odd-mass nuclei, are given in Table II.

TABLE II. Composition of the IBFM wave functions corresponding to the low-energy positive-parity states of the studied odd-mass Kr nuclei (in percent units).

$^{87}\text{Kr}$					$^{89}\text{Kr}$			
$J$	$3s_{1/2}$	$2d_{3/2}$	$2d_{5/2}$	$1g_{7/2}$	$3s_{1/2}$	$2d_{3/2}$	$2d_{5/2}$	$1g_{7/2}$
$1/2_1^+$	41	5	54	0	43	8	48	1
$3/2_1^+$	11	23	62	4	4	6	89	1
$3/2_2^+$	29	11	58	3	20	34	36	11
$5/2_1^+$	4	1	95	0	6	3	90	1
$5/2_2^+$	7	0	92	0	20	3	76	1
$7/2_1^+$	1	1	95	3	1	2	92	5
$9/2_1^+$	5	1	94	0	7	2	91	0
$11/2_1^+$	1	1	95	3	5	1	94	0

$^{91}\text{Kr}$				$^{93}\text{Kr}$				
$J$	$3s_{1/2}$	$2d_{3/2}$	$2d_{5/2}$	$1g_{7/2}$	$3s_{1/2}$	$2d_{3/2}$	$2d_{5/2}$	$1g_{7/2}$
$1/2_1^+$	49	35	6	10	17	46	30	7
$3/2_1^+$	7	56	6	31	58	21	10	11
$3/2_2^+$	9	6	83	2	50	27	11	12
$5/2_1^+$	5	2	92	1	21	43	30	6
$5/2_2^+$	40	38	8	14	45	24	25	7
$7/2_1^+$	4	37	0	59	60	19	5	16
$9/2_1^+$	12	6	76	6	49	21	26	3
$11/2_1^+$	3	32	0	65	60	22	3	16

$^{95}\text{Kr}$				
$J$	$3s_{1/2}$	$2d_{3/2}$	$2d_{5/2}$	$1g_{7/2}$
$1/2_1^+$	11	48	36	5
$3/2_1^+$	46	25	6	23
$3/2_2^+$	39	32	9	20
$5/2_1^+$	12	44	36	7
$5/2_2^+$	42	21	20	17
$7/2_1^+$	44	23	4	29
$9/2_1^+$	16	41	35	8
$11/2_1^+$	42	24	2	32

#### 1. $^{87}\text{Kr}$

Figure 4 depicts the energy spectra for  $^{87}\text{Kr}$ . The experimental results are well reproduced within our approach. As can be seen from Table II, 95 % of the wave function of the  $5/2_1^+$  ground state is accounted for by the  $2d_{5/2}$  single-particle orbital coupled to the even-even nucleus  $^{86}\text{Kr}$ . For both, the  $1/2_1^+$  and  $3/2_1^+$  wave functions the  $3s_{1/2}$ ,  $2d_{3/2}$  and  $2d_{5/2}$  configurations have a stronger mixing.

#### 2. $^{89}\text{Kr}$

The experimental information is very scarce for  $^{89}\text{Kr}$ . Its ground state has been tentatively assigned to  $J^\pi = 3/2^+$  and a  $5/2^+$  level has been found just 29 keV above it. Moreover, this  $5/2^+$  state and the  $9/2^+$  one at 982 keV, have been interpreted [36] as the members of the  $\Delta J = 2$  band based on the neutron  $2d_{5/2}$  orbital coupled to the  $^{90}\text{Kr}$  core. Our calculations predict the  $3/2_1^+$ ,

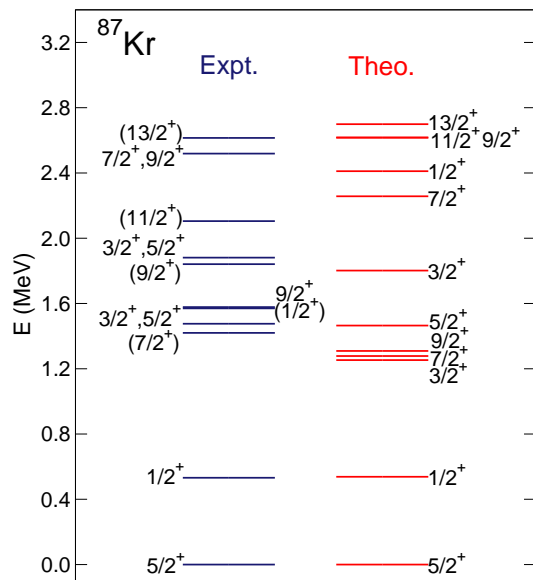


FIG. 4. (Color online) The low-lying positive-parity excitation spectrum obtained for the nucleus  $^{87}\text{Kr}$  is compared with the available experimental data Ref. [36]. Energy levels in parenthesis have not been established experimentally.

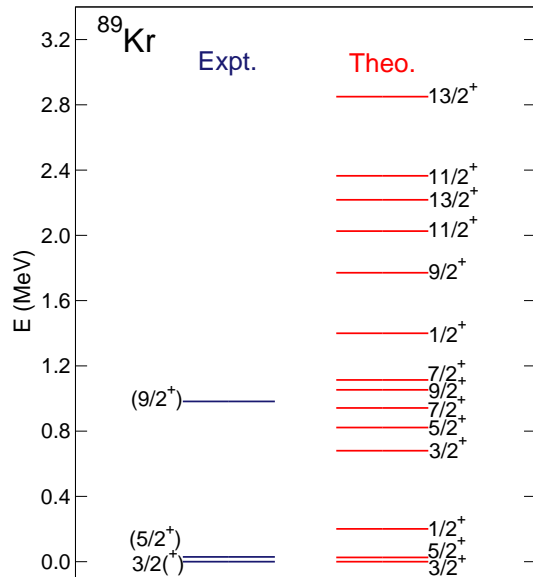


FIG. 5. (Color online) The same as in Fig. 4, but for  $^{89}\text{Kr}$ . Experimental data have been taken from Ref. [36].

$5/2_1^+$  and  $9/2_1^+$  states to be mainly ( $\approx 90\%$ ) composed of the  $2d_{5/2}$  configuration (see, Table II). Due to the large overlaps between their wave functions, large E2 matrix elements have been obtained for the  $5/2_1^+ \rightarrow 3/2_1^+$  and  $9/2_1^+ \rightarrow 5/2_1^+$  transitions [see, Figs. 9 panel (d) and 9 panel (e)].

### 3. $^{91}\text{Kr}$

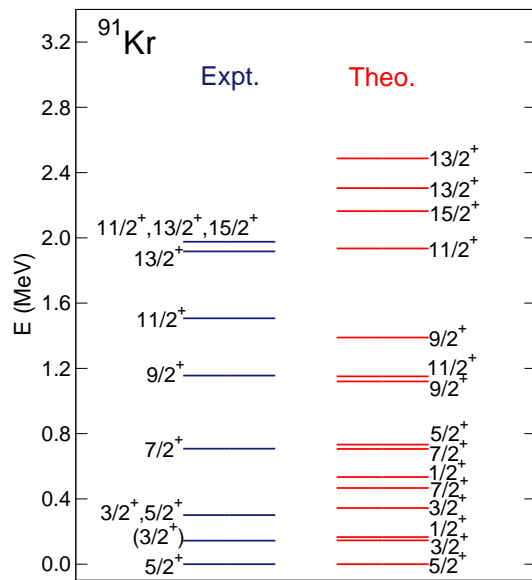


FIG. 6. (Color online) The same as in Fig. 4, but for  $^{91}\text{Kr}$ . Experimental data have been taken from Refs. [16, 36].

In the case of  $^{91}\text{Kr}$ , as seen from Fig. 6, our calculations reproduce well the experimental spectrum [16, 36] exception made of the  $7/2_1^+$  and  $11/2_1^+$  levels which are predicted to have a rather low excitation energy. From Table II, one observes that the wave functions of the  $5/2_1^+$  ground and the  $9/2_1^+$  states are similar, both dominated by the  $2d_{5/2}$  configuration. They are thus expected to be members of a  $\Delta J = 2$  band. Furthermore, the  $3/2_1^+$  state (see, Table II) seems to be the band head of the  $\Delta J = 2$  band with the members  $3/2_1^+$ ,  $7/2_1^+$ ,  $\dots$ . Consequently, as shown later in Fig. 9, rather large  $B(E2; 9/2_1^+ \rightarrow 5/2_1^+)$  and  $B(E2; 7/2_1^+ \rightarrow 3/2_1^+)$  transitions have been found for  $^{91}\text{Kr}$ .

In the case of  $^{91}\text{Kr}$ , our calculations reproduce the experimental results as well as the results of large-scale shell-model calculations [16]. However, within the shell model, neutrons predominantly occupy the  $2d_{5/2}$  orbital for all the observed states in  $^{91}\text{Kr}$ . This is somewhat at variance with our results where, the  $7/2_1^+$  state is composed of the  $2d_{3/2}$  (37 %) and  $1g_{7/2}$  (59 %) configurations (see, Table II).

### 4. $^{93}\text{Kr}$

For  $^{93}\text{Kr}$ , in Fig. 7, we conclude that the agreement with the experimental spectrum is reasonable. As in the case of  $^{91}\text{Kr}$ , the  $7/2_1^+$  and  $11/2_1^+$  levels are too low and the  $15/2_1^+$  excitation energy is overestimated. In this nucleus the ground state corresponds to  $J = 1/2^+$ . From

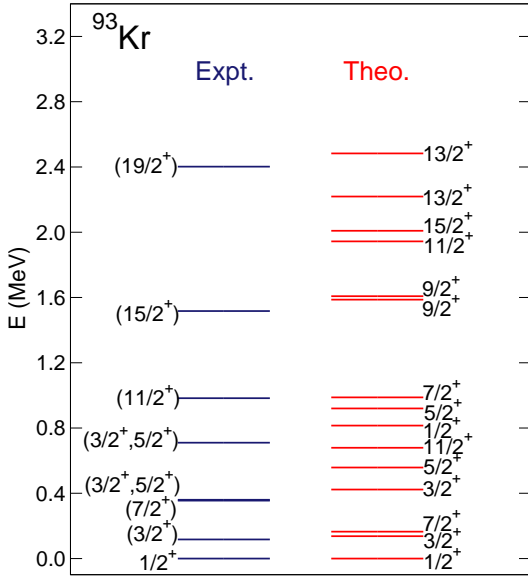


FIG. 7. (Color online) The same as in Fig. 4, but for  $^{93}\text{Kr}$ . Experimental data have been taken from Ref. [17, 36].

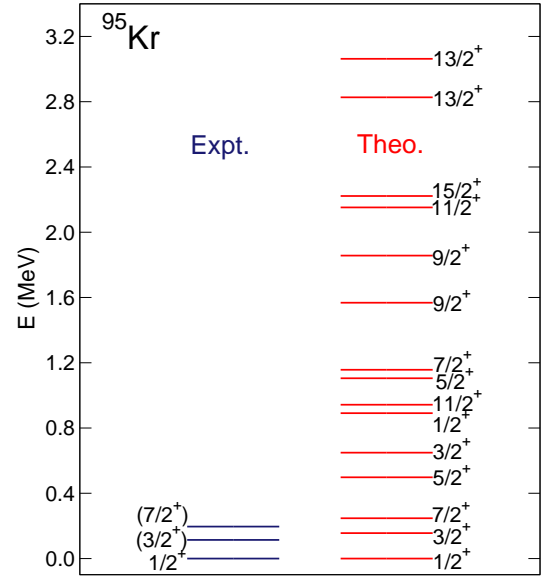


FIG. 8. (Color online) The same as in Fig. 4, but for  $^{95}\text{Kr}$ . Experimental data have been taken from Ref. [36].

the results shown in Table II, one realizes that in our calculations, the four single-particle configurations are significantly mixed in the  $J = 1/2_1^+$  ground states of  $^{93,95}\text{Kr}$ . This is in contrast with the  $^{87-91}\text{Kr}$  cases, where the ground states ( $J = 5/2_1^+$  for  $^{87,91}\text{Kr}$  and  $3/2_1^+$  for  $^{89}\text{Kr}$ ) are predominantly ( $\approx 90\%$ ) composed of the  $2d_{5/2}$  configuration,

### 5. $^{95}\text{Kr}$

In the case of  $^{95}\text{Kr}$ , the experimental information is even more scarce than for  $^{91,93}\text{Kr}$ . Here, the predicted spectrum resembles the one of  $^{93}\text{Kr}$ . From Table II we observe that the  $1/2_1^+$  ground state has a large overlap with the  $5/2_1^+$  state. Both are expected to form a  $\Delta J = 2$  band. On the other hand, the structural similarity between the  $3/2_1^+$  and  $7/2_1^+$  states suggests that they are members of another  $\Delta J = 2$  band.

### C. Electromagnetic properties

The experimental information on the electromagnetic transition rates of the studied odd-mass Kr isotopes is rather scarce. Moreover, our choice of effective charges, especially for the E2 transition operator, might not necessarily be the optimal one. Therefore, in this section we will only discuss the systematic of the  $B(E2)$  and  $B(M1)$  values between a few lowest states as functions of the nucleon number.

Figure 9 displays the  $B(E2)$  transition probabilities for both the  $\Delta J = 1$  and 2 transitions to the  $1/2_1^+$ ,

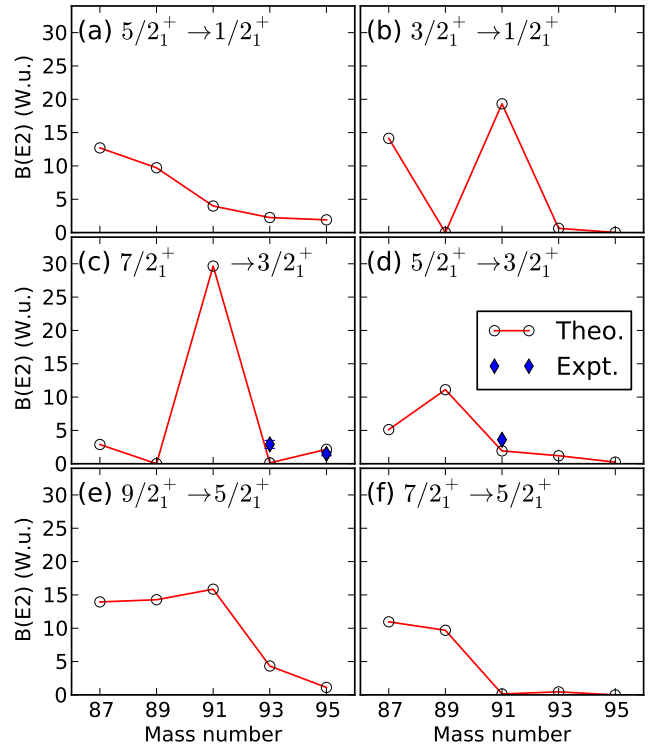


FIG. 9. (Color online) The  $B(E2)$  transition probabilities between the low-lying positive-parity yrast states for the odd-mass nuclei  $^{87-95}\text{Kr}$  are plotted, as functions of the mass number. The experimental data have been taken from Ref. [36].

$3/2_1^+$ , and  $5/2_1^+$  states. Most of the computed  $B(E2)$  values exhibit a gradual decrease as functions of the

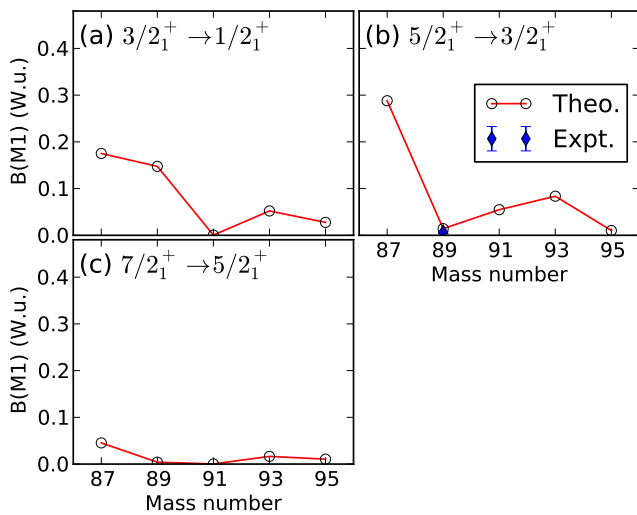


FIG. 10. (Color online) The same as in Fig. 9, but for the  $B(M1)$  rates.

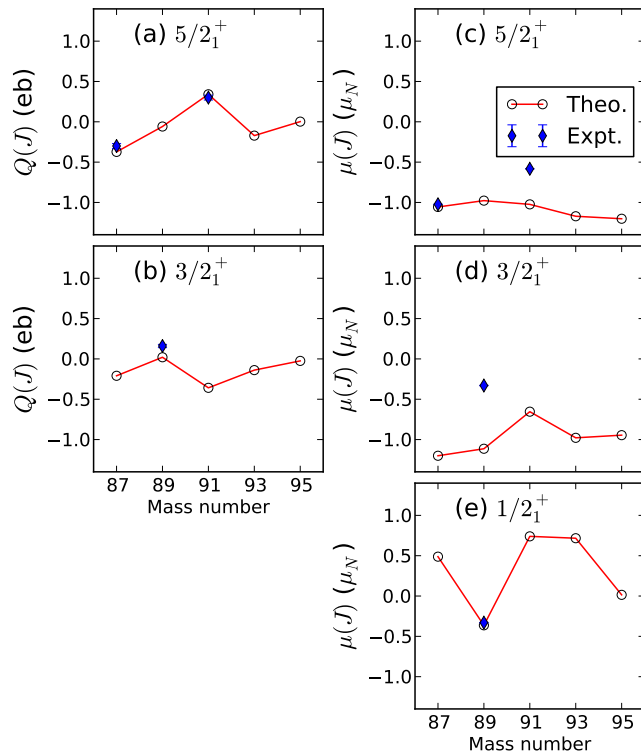


FIG. 11. (Color online) Spectroscopic quadrupole moments  $Q(J)$  and magnetic moments  $\mu(J)$  for the  $5/2_1^+$ ,  $3/2_1^+$  and  $1/2_1^+$  states of the odd-mass isotopes  $^{87-95}\text{Kr}$ . The experimental data have been taken from Ref. [38].

mass number. Nevertheless, the  $B(E2; 3/2_1^+ \rightarrow 1/2_1^+)$  and  $B(E2; 7/2_1^+ \rightarrow 3/2_1^+)$  values are especially large for the transitional nucleus  $^{91}\text{Kr}$  (see, Fig. 3). Especially, as

mentioned in Sec. IV B 3, the  $7/2_1^+$  and  $3/2_1^+$  states in  $^{91}\text{Kr}$  form the  $\Delta J = 2$  band that is connected by the particularly strong  $E2$  transitions in comparison to the adjacent nuclei. In the transitional nuclei around  $^{91}\text{Kr}$ , some  $B(E2)$  decay patterns should be sensitive to the detailed nuclear structure at low energy, and the irregularity such as those observed in Figs. 9(b) and 9(c) could easily occur. The  $B(M1)$  transition rates are depicted in Fig. 10.

A few experimental values are available [38] for the spectroscopic quadrupole  $Q(J)$  and magnetic  $\mu(J)$  moments. Those moments are plotted in Fig. 11 for the  $5/2_1^+$ ,  $3/2_1^+$  and  $1/2_1^+$  states. In most of the cases, they exhibit an irregular behavior around the  $^{89}\text{Kr}$  or  $^{91}\text{Kr}$ . Exception made of  $\mu(5/2_1^+)$  for  $^{91}\text{Kr}$  and  $\mu(3/2_1^+)$  for  $^{89}\text{Kr}$ , our calculations reproduce the experiment reasonably well.

## V. SUMMARY AND CONCLUDING REMARKS

In this paper, we have studied the spectroscopic properties of neutron-rich odd-mass isotopes  $^{87-95}\text{Kr}$  within the IBFM-2 framework based on the Gogny-D1M EDF. The  $(\beta, \gamma)$ -deformation energy surfaces for the even-even boson-core nuclei  $^{86-94}\text{Kr}$ , spherical single-particle energies and occupation probabilities of the odd-mass systems have been obtained using the constrained HFB approximation. Those quantities have then been employed as a microscopic input to obtain most of the parameters of the corresponding IBFM-2 Hamiltonian. The remaining parameters for the boson-fermion interaction have been fitted to the experimental spectrum for each odd-mass nucleus.

The evolution of the excitation spectra and electromagnetic properties for the studied odd-mass isotopes suggests a gradual change in the deformation of the corresponding intrinsic states. This agrees well with the shape/phase transition already observed in the neighboring even-even systems [6]. We have analyzed in detail the low-lying levels and the corresponding wave functions for each of the considered isotopes. Our results illustrate that the IBFM-2 framework, which has rarely been applied to this mass region, can be used as a computationally feasible tool to access the spectroscopic properties of neutron-rich odd-mass nuclei.

We have restricted ourselves to Kr isotopes with mass  $A \leq 95$ . This is partly because the experimental data, required to fit the boson-fermion parameters, are not yet available for larger mass numbers. On the other hand, a theoretical framework that couples odd-nucleon degrees of freedom to the IBM core, including intruder configurations associated with different intrinsic shapes, is still required to describe odd-mass systems beyond  $A = 96$  for which, shape coexistence is expected to play a key role. Work along these lines is in progress and will be reported elsewhere.

## ACKNOWLEDGMENTS

We thank Dr. A. Blazhev for valuable discussions. One of us (KN) acknowledges support by the QuantiX Lie Centre of Excellence, a project co-financed by the

Croatian Government and European Union through the European Regional Development Fund - the Competitiveness and Cohesion Operational Programme (Grant KK.01.1.1.01.0004). The work of LMR was supported by Spanish Ministry of Economy and Competitiveness (MINECO) Grant Nos. FPA2015-65929-P and FIS2015-63770-P.

- 
- [1] P. Cejnar, J. Jolie, and R. F. Casten, *Rev. Mod. Phys.* **82**, 2155 (2010).
- [2] K. Heyde and J. L. Wood, *Rev. Mod. Phys.* **83**, 1467 (2011).
- [3] T. Togashi, Y. Tsunoda, T. Otsuka, and N. Shimizu, *Phys. Rev. Lett.* **117**, 172502 (2016), URL <https://link.aps.org/doi/10.1103/PhysRevLett.117.172502>.
- [4] C. Kremer, S. Aslanidou, S. Bassauer, M. Hilcker, A. Krugmann, P. von Neumann-Cosel, T. Otsuka, N. Pietralla, V. Y. Ponomarev, N. Shimizu, et al., *Phys. Rev. Lett.* **117**, 172503 (2016), URL <https://link.aps.org/doi/10.1103/PhysRevLett.117.172503>.
- [5] E. Clément, M. Zielińska, S. Péru, H. Goutte, S. Hilaire, A. Gørgen, W. Korten, D. T. Doherty, B. Bastin, C. Bauer, et al., *Phys. Rev. C* **94**, 054326 (2016), URL <https://link.aps.org/doi/10.1103/PhysRevC.94.054326>.
- [6] M. Albers, N. Warr, K. Nomura, A. Blazhev, J. Jolie, D. Mücher, B. Bastin, C. Bauer, C. Bernards, L. Bettermann, et al., *Phys. Rev. Lett.* **108**, 062701 (2012).
- [7] S. Naimi, G. Audi, D. Beck, K. Blaum, C. Böhm, C. Borgmann, M. Breitenfeldt, S. George, F. Herfurth, A. Herlert, et al., *Phys. Rev. Lett.* **105**, 032502 (2010), URL <https://link.aps.org/doi/10.1103/PhysRevLett.105.032502>.
- [8] M. Albers, K. Nomura, N. Warr, A. Blazhev, J. Jolie, D. Mcher, B. Bastin, C. Bauer, C. Bernards, L. Bettermann, et al., *Nuclear Physics A* **899**, 1 (2013), ISSN 0375-9474, URL <http://www.sciencedirect.com/science/article/pii/S0375947413000237>.
- [9] J. Dudouet, A. Lemasson, G. Duchêne, M. Rejmund, E. Clément, C. Michelagnoli, F. Didierjean, A. Korichi, G. Maquart, O. Stezowski, et al., *Phys. Rev. Lett.* **118**, 162501 (2017), URL <https://link.aps.org/doi/10.1103/PhysRevLett.118.162501>.
- [10] F. Flavigny, P. Doornenbal, A. Obertelli, J.-P. Delaroche, M. Girod, J. Libert, T. R. Rodriguez, G. Authalet, H. Baba, D. Calvet, et al., *Phys. Rev. Lett.* **118**, 242501 (2017), URL <https://link.aps.org/doi/10.1103/PhysRevLett.118.242501>.
- [11] R. Rodríguez-Guzmán, P. Sarriguren, L. M. Robledo, and S. Perez-Martin, *Phys. Lett. B* **691**, 202 (2010).
- [12] T. R. Rodríguez, *Phys. Rev. C* **90**, 034306 (2014).
- [13] J. Xiang, J. M. Yao, Y. Fu, Z. H. Wang, Z. P. Li, and W. H. Long, *Phys. Rev. C* **93**, 054324 (2016), URL <https://link.aps.org/doi/10.1103/PhysRevC.93.054324>.
- [14] K. Nomura, R. Rodríguez-Guzmán, and L. M. Robledo, *Phys. Rev. C* **94**, 044314 (2016), URL <https://link.aps.org/doi/10.1103/PhysRevC.94.044314>.
- [15] K. Nomura, R. Rodríguez-Guzmán, Y. M. Humadi, L. M. Robledo, and H. Abusara, *Phys. Rev. C* **96**, 034310 (2017), URL <https://link.aps.org/doi/10.1103/PhysRevC.96.034310>.
- [16] T. Rzaca-Urban, K. Sieja, W. Urban, M. Czerwiński, A. Blanc, M. Jentschel, P. Mutti, U. Köster, T. Soldner, G. de France, et al., *Phys. Rev. C* **95**, 064302 (2017), URL <https://link.aps.org/doi/10.1103/PhysRevC.95.064302>.
- [17] J. K. Hwang, A. V. Ramayya, J. H. Hamilton, S. H. Liu, N. T. Brewer, Y. X. Luo, J. O. Rasmussen, S. J. Zhu, and R. Donangelo, *Phys. Rev. C* **82**, 034308 (2010), URL <https://link.aps.org/doi/10.1103/PhysRevC.82.034308>.
- [18] J. Genevey, R. Guglielmini, R. Orlandi, J. A. Pinston, A. Scherillo, G. Simpson, I. Tsekhanovich, N. Warr, and J. Jolie, *Phys. Rev. C* **73**, 037308 (2006), URL <https://link.aps.org/doi/10.1103/PhysRevC.73.037308>.
- [19] A. Bohr, *Mat. Fys. Medd. Dan. Vid. Selsk.* **27**, 16 (1953).
- [20] P. Ring and P. Schuck, *The nuclear many-body problem* (Berlin: Springer-Verlag, 1980).
- [21] S. Perez-Martin and L. M. Robledo, *Phys. Rev. C* **78**, 014304 (2008), URL <https://link.aps.org/doi/10.1103/PhysRevC.78.014304>.
- [22] R. Rodríguez-Guzmán, P. Sarriguren, and L. M. Robledo, *Phys. Rev. C* **82**, 044318 (2010).
- [23] R. Rodríguez-Guzmán, P. Sarriguren, and L. M. Robledo, *Phys. Rev. C* **82**, 061302 (2010).
- [24] K. Nomura, T. Nikšić, and D. Vretenar, *Phys. Rev. C* **93**, 054305 (2016).
- [25] F. Iachello and P. Van Isacker, *The interacting boson-fermion model* (Cambridge University Press, Cambridge, 1991).
- [26] K. Nomura, R. Rodríguez-Guzmán, and L. M. Robledo, *Phys. Rev. C* **96**, 014314 (2017), URL <https://link.aps.org/doi/10.1103/PhysRevC.96.014314>.
- [27] K. Nomura, R. Rodríguez-Guzmán, and L. M. Robledo, *Phys. Rev. C* **96**, 064316 (2017), URL <https://link.aps.org/doi/10.1103/PhysRevC.96.064316>.
- [28] F. H. Al-Khudair, *Phys. Rev. C* **91**, 054304 (2015), URL <https://link.aps.org/doi/10.1103/PhysRevC.91.054304>.
- [29] T. Otsuka, A. Arima, and F. Iachello, *Nucl. Phys. A* **309**, 1 (1978).
- [30] R. Rodríguez-Guzmán, P. Sarriguren, L. M. Robledo, and J. E. García-Ramos, *Phys. Rev. C* **81**, 024310 (2010).
- [31] J. Decharge and M. Girod and D. Gogny, *Phys. Lett. B* **55**, 361 (1975).
- [32] S. Goriely, S. Hilaire, M. Girod, and S. Péru, *Phys. Rev. Lett.* **102**, 242501 (2009).
- [33] K. Nomura, N. Shimizu, and T. Otsuka, *Phys. Rev. Lett.* **101**, 142501 (2008).
- [34] K. Nomura, N. Shimizu, and T. Otsuka, *Phys. Rev. C* **81**, 044307 (2010).

- [35] O. Scholten, *Prog. Part. Nucl. Phys.* **14**, 189 (1985).
- [36] Brookhaven National Nuclear Data Center,  
<http://www.nndc.bnl.gov>.
- [37] F. Iachello and A. Arima, *The interacting boson model*  
(Cambridge University Press, Cambridge, 1987).
- [38] N. Stone, *At. Data Nucl. Data Tables* **90**, 75 (2005).